

Band Structure and Exciton Dynamics in Quasi-2D Dodecylammonium Halide Perovskites

Giuseppe Ammirati, Faustino Martelli, Patrick O’Keeffe, Stefano Turchini, Alessandra Paladini, Maurizia Palummo, Giacomo Giorgi, Marco Cinquino, Milena De Giorgi, Luisa De Marco, and Daniele Catone*

Femtosecond transient absorption spectroscopy (FTAS) is an important tool to investigate the physics of halide perovskites having different dimensionality, morphology, and architectures, giving insights into the electronic and excitonic optical transitions. Here, FTAS on monolayer ($n = 1$) and multilayer ($n = 2, 3$) quasi-2D perovskites in the Ruddlesden–Popper phase: $\text{DA}_2\text{MA}_{n-1}\text{Pb}_{n+1}\text{I}_{3n+1}$ (DAMAPI) is presented, with the dodecylammonium ($\text{DA} = \text{CH}_3-(\text{CH}_2)_{11}-\text{NH}_3^+$) as the spacer and methylammonium ($\text{MA} = \text{CH}_3\text{NH}_3^+$) as the organic cation for samples with $n > 1$. The measurements, performed at 77 K and room temperature using several pump energies and excitation densities, allow the observation of different absorption bleaching energies. Those energies are compared with the results of first-principles theoretical simulations based on density functional theory, the GW method, and the Bethe–Salpeter equation and assigned to transitions involving excitons with principal quantum numbers 1s and 2s. The temporal analysis of the absorption bleaching indicates the exciton–exciton annihilation as the main relaxation mechanism in the first picoseconds after excitation, while exciton radiative recombination is observed at longer time delays (>100 ps). Therefore, FTAS allows the study of the carrier dynamics and, given its high sensitivity to carrier density changes, the observation of spectral features not observable with steady-state measurements.

1. Introduction


Quasi-2D perovskites in the Ruddlesden–Popper phase are currently being studied extensively for their good optoelectronic performances^[1–3] and chemical stability,^[4,5] which lead them to be among the best candidates for new active materials in optoelectronic applications such as photovoltaic^[5–7] and light-emitting devices.^[8,9] Ruddlesden–Popper Perovskites (RPPs) consist of self-assembled multiple perovskite layers sandwiched between organic spacers having the stoichiometric formula $\text{R}_2\text{A}_{n-1}\text{B}_1\text{X}_{3n+1}$, where n is the number of perovskite sheets, A and B are the cations, X is the anion and R is the organic molecule that acts as the spacer. As one of the major advantages over the usual tridimensional perovskites, RPPs show higher stability because of the hydrophobic character of the organic spacer, which prevents the absorption of moisture, the main degradation mechanism of perovskites.^[4]

G. Ammirati, S. Turchini, D. Catone
 Istituto di Struttura della Materia – CNR (ISM-CNR)
 EuroFEL Support Laboratory (EFSL)
 Via del Fosso del Cavaliere 100, Rome 00133, Italy
 E-mail: daniele.catone@cnr.it

G. Ammirati
 CHOSE (Centre for Hybrid and Organic Solar Energy)
 Department of Electronic Engineering
 University of Rome Tor Vergata
 Via del Politecnico 1, Rome 00133, Italy

F. Martelli
 Istituto per la Microelettronica e i Microsistemi (IMM)
 CNR
 Rome I-00133, Italy

P. O’Keeffe, A. Paladini
 Istituto di Struttura della Materia – CNR (ISM-CNR)
 EuroFEL Support Laboratory (EFSL)
 Monterotondo Scalo 00015, Italy

 The ORCID identification number(s) for the author(s) of this article can be found under <https://doi.org/10.1002/adom.202201874>.

© 2023 The Authors. Advanced Optical Materials published by Wiley-VCH GmbH. This is an open access article under the terms of the Creative Commons Attribution License, which permits use, distribution and reproduction in any medium, provided the original work is properly cited.

DOI: 10.1002/adom.202201874

M. Palummo
 INFN
 Dept of Physics
 University of Rome Tor Vergata
 Via della Ricerca Scientifica 1, Roma 00133, Italy

G. Giorgi
 Department of Civil & Environmental Engineering (DICA)
 University of Perugia
 Perugia I-06123, Italy

G. Giorgi
 CNR-SCITEC
 Perugia I-06123, Italy

G. Giorgi
 CIRIAF – Interuniversity Research Centre
 University of Perugia
 Via G. Duranti 63, Perugia 06125, Italy

M. Cinquino, M. De Giorgi, L. De Marco
 CNR NANOTEC
 Institute of Nanotechnology
 c/o campus Ecotekne
 University of Salento
 Via Monteroni, Lecce 73100, Italy

M. Cinquino
 Dipartimento di Matematica e Fisica E. De Giorgi
 Università Del Salento
 Campus Ecotekne, Via Monteroni, Lecce 73100, Italy

Furthermore, RPPs permit a huge structural diversity because the organic spacer leads to less tight constraints due to the Goldschmidt tolerance factor.^[10]

The reduced dielectric screening and the quantum confinement in a monolayer of RPP materials generate large bandgaps and stable excitons at room temperature with binding energies of the order of hundreds of meV^[3,11–15] as seen in other 2D semiconductors.^[16,17] Moreover, the physical properties of RPPs are strongly influenced by the number of layers that affects the electronic bandgap and the exciton binding energy which decreases as the number of layers increases.^[18] These properties are also correlated with the chemical composition and the structure of the organic spacer used as the interlayer material. In fact, the reduction of the bond length of B-X-B and the change of their bond angle induce a modification of the optical bandgap that is directly correlated with the steric hindrance of the organic spacer.^[18–20] Furthermore, the correct choice of the organic spacer is essential to obtain good quality crystallization of the 2D material^[21,22] and permits the film quality to be optimized,^[23] the crystal orientation to be tuned^[24] and the stability of the system to be improved.^[4,25] The flexibility of these RPP materials in tuning their optoelectronic properties by controlling the number of perovskite layers and by choosing the appropriate organic spacer, makes them particularly suitable for several applications in the field of photovoltaics^[23,26–28] and as light emitters.^[29–32] It has recently been discovered that a mixture of layered 2D perovskites can be engineered to better balance light absorption and/or charge carriers transport in solar cells in order to increase the conversion efficiency.^[33]

Femtosecond Transient Absorption Spectroscopy (FTAS), a pump-probe technique, has proven to be an important tool to investigate the ultrafast physics of halide perovskites with different dimensionalities,^[34–36] morphologies and architectures.^[37] FTAS gives information on the charge carrier generation, recombination, and many-body interaction by studying the evolution of the transient signal as a function of the time delay between the pump and the probe. Moreover, the spectral and temporal analyses of the transient signal give insights into the band structure and the electronic states involved in the photoexcitation process, interpreting the energy positions and the relative intensities of the negative and positive signals that characterize the typical derivative-like transient response of RPP materials.^[38–40] Previous investigations on the charge carrier dynamics in 2D perovskites by ultrafast time-resolved spectroscopies provide information on the lifetime and the diffusion length of the charge carriers,^[41,42] on the hot carriers cooling,^[43,44] on the role of the organic cations and the number of inorganic layers in governing the ultrafast charge carrier dynamics^[45] and on the charge transfer processes.^[33,44] A transient absorption microscopy experiment has shown the occurrence in 2D perovskites of a slow exciton–exciton annihilation (EEA),^[46] which is a non-radiative many-body interaction, a form of Auger recombination where the kinetic energy of an exciton is transferred to another exciton.^[47] This non-radiative channel, which is still not completely and extensively studied, is strictly connected to the exciton energetics and more in general to the optoelectronic properties of 2D perovskite materials.

In this work, we report FTAS measurements on the RPP monolayer ($n = 1$) and multilayer ($n = 2, 3$) of quasi-2D

perovskites $\text{DA}_2\text{MA}_{n-1}\text{Pb}_n\text{I}_{3n+1}$ (DAMAPI), with the dodecylammonium ($\text{DA} = \text{CH}_3(\text{CH}_2)_{11}\text{NH}_3^+$) as the spacer and methylammonium ($\text{MA} = \text{CH}_3\text{NH}_3^+$) as the organic cation for samples with $n > 1$. DA was selected as the organic spacer because it allows the formation of a stable 2D RPP due to the strong van der Waals interactions between adjacent DA molecules which also induce high hydrophobicity and resistance to moisture thanks to their long aliphatic chain.^[48]

The measurements were performed at 77 K and room temperature (RT) using several pump energies and excitation densities, allowing the observation of absorption bleaching energies corresponding to different excitonic and electronic transitions in DAMAPI. The values of those energies are compared with the results of first-principles theoretical simulations based on Density Functional Theory (DFT), the GW method, and the Bethe–Salpeter Equation (BSE) to estimate the role of many-body effects, such as band-gap renormalization, and excitonic effects. The temporal analysis of the absorption bleaching of the excitonic transitions indicates that the EEA process is the main relaxation mechanism in the first picoseconds after the excitation, while exciton radiative recombination is observed at longer time delays. Our work represents a first attempt to combine experimental and theoretical investigations of the excitons in 2D and quasi-2D hybrid perovskites.

2. Materials and Methods

2.1. Materials Growth

The preparation of the DAMAPI ($\text{DA}_2\text{MA}_{n-1}\text{Pb}_n\text{I}_{3n+1}$) samples with different layer size ($n = 1, 2, 3$), **Figure 1**, is described by the following synthesis process.^[48,49]

$(\text{DA})_2\text{PbI}_4$ ($n = 1$) single crystals were prepared as follows: 230.5 mg of lead iodide (PbI_2) and 313.26 mg of *n*-dodecylammonium iodide ($\text{C}_{12}\text{H}_{25}\text{NH}_3\text{I}$) were dissolved in 1 mL γ -Butyrolactone (GBL) and stirred at 343.15 K for 1 h. The precursor solution was prepared in an N_2 -filled glovebox. Quartz substrates were cleaned with acetone and water in an ultrasonic bath for 10 min each and then soaked into a TL1 washing solution ($\text{H}_2\text{O}_2/\text{NH}_3/\text{H}_2\text{O}$ 5:1:1, v/v), heated at 353.15 K for 10 min to remove organic contamination and finally rinsed ten times in water. The perovskite solution (1 μL) was deposited on the top of the substrate and immediately covered by a second substrate. Then, a small vial containing 2 mL of diethyl ether was placed on top of the two sandwiched substrates. Substrates and vials were placed in a bigger Teflon vial, closed with a screw cap, and left undisturbed. After 2 days millimeter-sized crystals appeared in between the two substrates having a thickness varying from a few to ten micrometers. $(\text{DA})_2(\text{MA})\text{Pb}_2\text{I}_7$, and $(\text{DA})_2(\text{MA})_2\text{Pb}_3\text{I}_{10}$ ($n = 2$ and 3 respectively) were synthesized using a new method where crystallization was induced by cooling down the solution. PbI_2 (447 mg), 74 mg of *n*-dodecylammonium iodide, and 693.9 mg of methylammonium iodide ($\text{CH}_3\text{NH}_3\text{I}$) were dissolved at 343.15 K in a mix of water/acetonitrile (1.05 per 1 mL respectively). Different amounts of potassium iodide (1045 mg for $n = 2$ and 161 mg for $n = 3$, respectively) were added to the solution to control the value of n . All the precursors were stirred at 343.15 K for 1 h producing a bright yellow

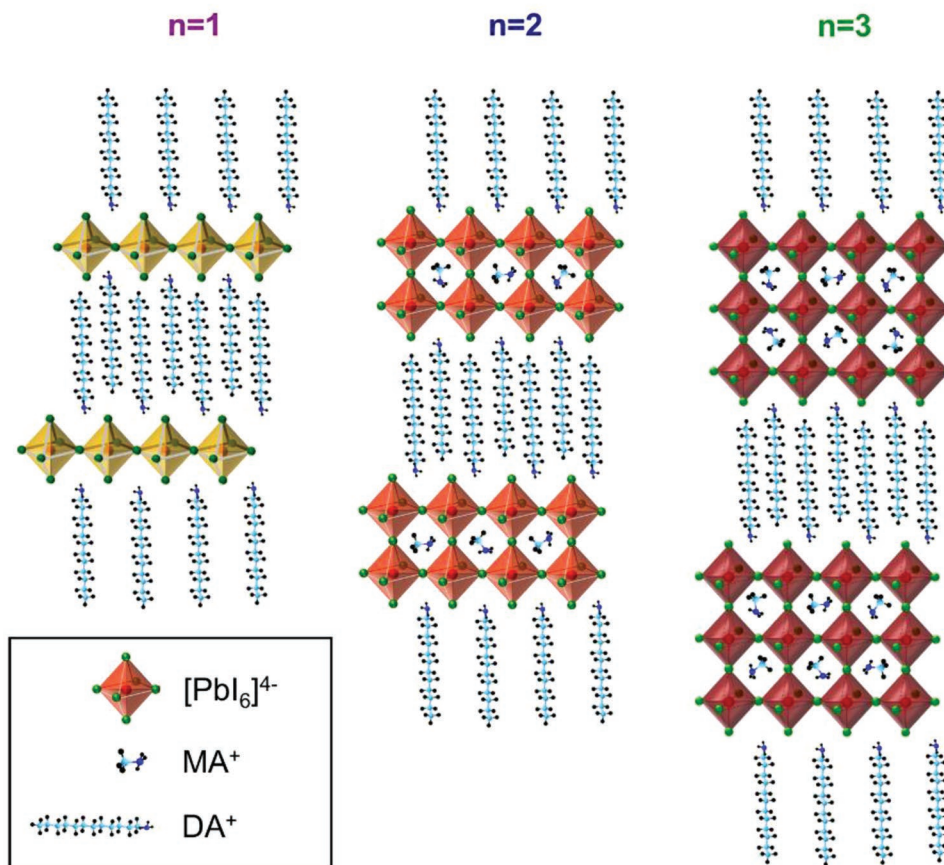


Figure 1. Schematic representation of $\text{DA}_2\text{MA}_{n-1}\text{PbI}_{3n+1}$ crystal structure for $n = 1, 2, 3$.^[48,49]

solution. Perovskite single crystals were then grown by storing the bright solution at room temperature. After 1 h at room temperature, small nuclei appear at different positions at the bottom of the vial. Then they started to grow into large-high-quality single crystals. After some hours (3 and 8 for $n = 2$ and $n = 3$, respectively), crystals at the bottom of the vial became thick and cm-sized platelets. Crystals were extracted using a net and then gently harvested and dried with paper to remove the remaining perovskite solution. Finally, crystals were carefully stored in the glovebox. All the solution synthesis procedures were performed in air. Optical microscopy images for DAMAPI samples are reported in Figure S1 (Supporting Information). The crystal structure and purity of the as-grown 2D perovskite single crystals were confirmed by synchrotron X-ray diffraction (XRD) analysis. Measurements on $(\text{DA})_2\text{PbI}_4$ and $(\text{DA})_2(\text{MA})\text{PbI}_7$ single crystals (respectively $n = 1$ and $n = 2$) were carried out at room temperature. This experiment has demonstrated that $n = 1$ 2D perovskites are orthorhombic having the $[\text{PbI}_6]^{4-}$ octahedra rotated one to each other, while $n = 2$ 2D perovskites are tetragonal.^[49]

2.2. Transient Absorption Measurements

FTAS measurements were performed using an amplified femtosecond laser system (35 fs pulse duration, 1 kHz repetition

rate, 4 W power centered at 800 nm) that generates the tunable pump pulses by using an optical parametric amplifier. The probe was a white light supercontinuum beam (360–780 nm) that was generated by focusing 3 μJ of the 800 nm pulse into a rotating CaF_2 crystal. The pump and the probe beams were focused on the sample with a diameter of 200 and 150 μm , respectively, and the delay time between the two was changed by modifying the optical path of the probe, resulting in an instrument response function of about 50 fs. The samples were investigated in a vacuum at 77 K and at RT. More details can be found elsewhere.^[50,51]

2.3. Theoretical Tools

Starting from available experimental structural data of RPP $n = 1$ (DAMAPI-1)^[49] its atomic structure was optimized by means of DFT calculations with the VASP code.^[52–55]

We used the electronic exchange-correlation functional of Perdew–Burke–Ernzerhof (PBE)^[56] along with the DFT-D3 dispersion correction to include the van der Waals interactions.^[57,58] The projector augmented wave (PAW) method was exploited together with a plane-wave basis set a cut-off of 400 eV, while the structures were considered converged when the residual forces were lower than 0.04 eV \AA^{-1} . During the optimization of the structural parameters, the Brillouin Zone

(BZ) of the large cell of DAMAPI-1 (348 atoms) were sampled by using the Γ point. All the electronic features were calculated by explicitly including the relativistic effects (SOC) due to the presence of heavy atoms (Pb, I).

Parallel to the calculations on DAMAPI-1, a simplified system was modeled whose atomic structure was obtained starting from the fully relaxed DAMAPI-1 atomic positions and unit cell, replacing the DA spacer organic cations with Cs cations to form Cs_2PbI_4 .^[59] Due to the drastic reduction of atoms in the cell (from 348 to 28) the many-body excited-state (GW and BSE) simulations become in this way computationally affordable. In this latter system a further relaxation run was then performed, keeping both atomic positions of the PbI_4 layers and the optimized lattice parameters of pristine DAMAPI-1 fixed, in order to preserve the correct structural distortion of the inorganic component. Still for such model system, by means of the Quantum-Espresso^[60,61] suite, the DFT calculations were repeated using the same xc-functional approximation exploited in the initial VASP optimization, norm conserving fully relativistic pseudopotentials with a kinetic energy cut-off of 120 Ry. In this way, the convergence of the structure was checked in terms of residual, minimal forces, improved the BZ sampling to calculate the electronic band structure (40 k -points), and also generated the KS eigenstates/values for the many-body code Yambo^[62,63] to determine the role of electronic correlation effects.

Similarly, the Quantum-Espresso suite was used to generate the Kohn-Sham (KS) eigenstates/values to perform the many-body analysis by means of the code Yambo^[62,63] and to get the quasi-particle (QP) energies in the GW approximation and the optical excitation energies and spectra solving the BSE.^[64–68] In this latter case, a Γ -centered $10 \times 10 \times 2$ ($14 \times 14 \times 2$) mesh was used for self-consistent (non-self-consistent) calculations. Differently from previously published works on similar systems,^[12–14] here the one-shot perturbative G_0W_0 was used to reduce the computational burden. The plasmon-pole approximation for the calculation of the inverse dielectric matrix, 81 eV (408 eV) was used for the correlation part of the self-energy Σ_c (exchange, Σ_x). Unoccupied states were summed up to 22 eV above the valence band maximum. It is clear for recent results that, in the framework of MBPT, report real-time exciton dynamics simulations including nuclear motion^[69–71] and also that other notable examples of real-time ab initio exciton dynamics simulations based on the time-dependent Kohn-Sham (TDKS) equation combined with Ehrenfest dynamics,^[72–74] or surface-hopping^[75,76] have been reported recently in the literature. Nevertheless, the approach was extremely suitable for the purposes of the present work since, in contrast to previously employed methods, it included electron-hole interactions, which were fundamental to correctly describe excited states of low-dielectric screening materials such as the 2D perovskites studied here.

3. Results and Discussion

Figure 2 shows the normalized absorption and photoluminescence (PL) spectra of the DAMAPI- n samples with $n = 1, 2, 3$ (respectively in violet, blue and green) acquired at room tem-

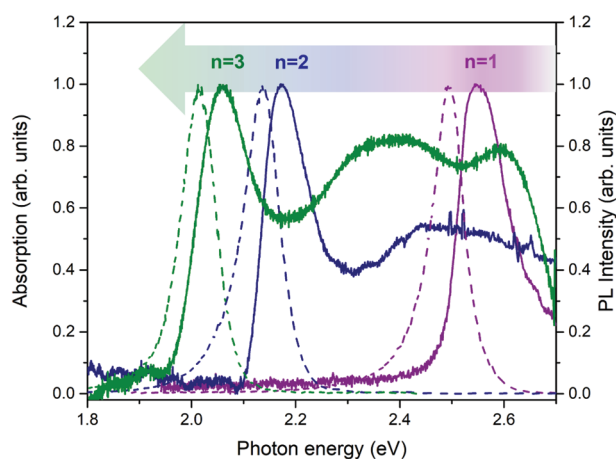


Figure 2. $\text{DA}_2\text{MA}_{n-1}\text{Pb}_n\text{I}_{3n+1}$ absorption (solid lines) and PL (dashed lines) spectra obtained at room temperature for $n = 1, 2, 3$ respectively in violet, blue, and green.

perature. The absorption spectra (solid lines) show an intense peak centered at 2.55 eV ($n = 1$), 2.17 eV ($n = 2$), and 2.06 eV ($n = 3$) corresponding to the respective exciton transitions. The strong redshift of the excitonic absorption energies with the number of perovskite layers is the overall result of the reduced quantum confinement and dielectric screening induced by the increase of the thickness of the quasi-2D material. PL spectra (dashed lines) show a single peak in the PL spectra indicating the emission of the exciton ground state.

Figure 3 shows the transient absorption (TA) spectra of DAMAPI-1 acquired at selected time delays ($t = 0.1, 0.2, 0.5, 1.0, 2.0, 5.0,$ and 10.0 ps) with a pump photon energy of $E_p = 3.35$ eV and a fluence of $220 \mu\text{J cm}^{-2}$ at RT (Figure 3a) and at 77 K (Figure 3b). The TA spectra obtained at RT show an intense negative signal at 2.51 eV assigned to the photobleaching (PB1) of the excitonic resonance, and a corresponding positive signal at higher energies due to a photoinduced absorption (PIA) of the probe. This derivative-like line shape is typical of the transient response of quasi-2D materials and is determined by different dynamical processes that take place under pump excitation such as band gap renormalization (BGR) and exciton screening due to the exciton-exciton and exciton-charge interactions. The scheme reported in Figure 3c depicts how the photogeneration of carriers by pump absorption modifies the electronic occupation, inducing additional screening effects and charge density variation.^[77] The carrier excitation leads to a BGR and to a reduction of the exciton binding energy (E_b) due to the screening of the Coulomb attraction of electrons and holes. As a result, the electronic bandgap (E_g) shrinks under photon excitation (E_g') leading to a redshift of the optical absorption ($\Delta E_g = E_g' - E_g$) while, on the other hand, the reduction of the exciton binding energy (E_b'), induces a blueshift ($\Delta E_b = E_b' - E_b$) in the optical absorption. The overall effect is a shift (δ) of the excitonic absorption resonance (ω) to an energy ($\omega = \omega + \delta$) that takes into account both the competitive renormalization effects, i.e., $\delta = |\Delta E_b| - |\Delta E_g|$. Therefore, the absorption resonance shift induces both a PB and a PIA around the excitonic resonance, as represented in Figure 3c. It is also important to note that the intensity, the shape and the minimum energy value of PB1 are

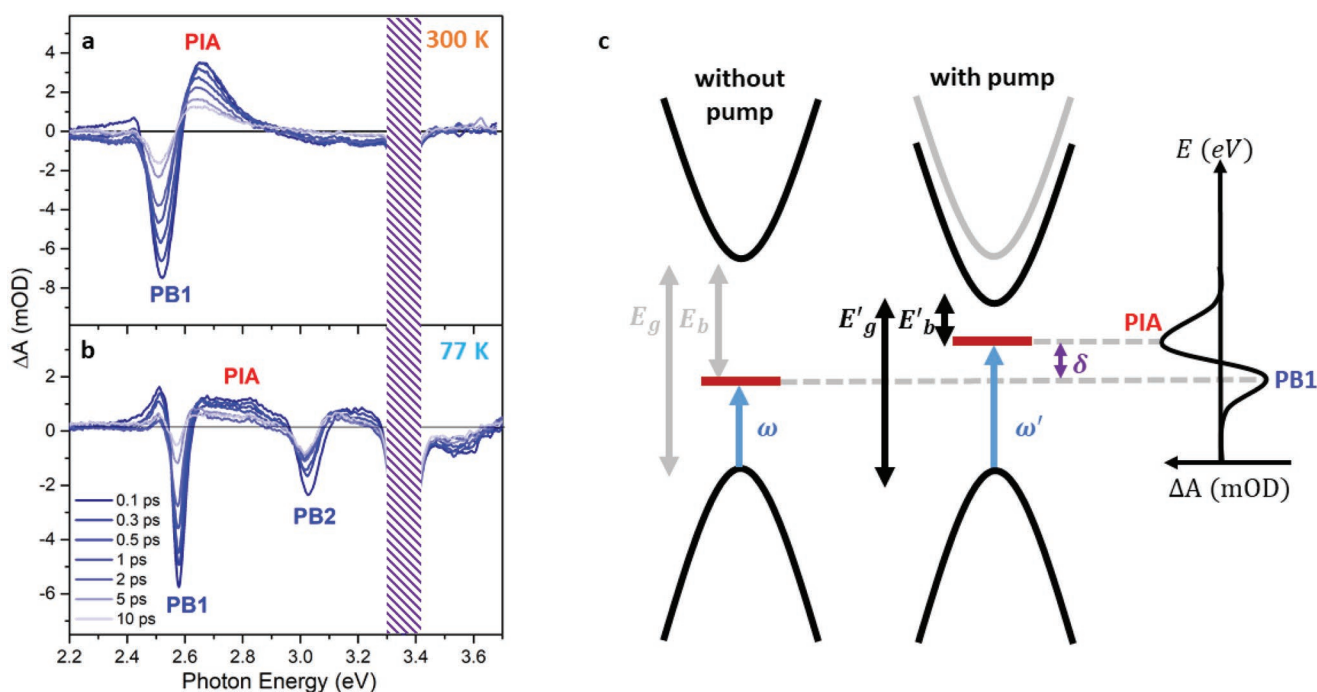


Figure 3. TA spectra of DAMAPI-1 acquired at selected time delays with $E_p = 3.35$ eV and $F = 220 \mu\text{J cm}^{-2}$ a) at room temperature and b) at 77 K. The labels (PB1, PB2, and PIA) used in the figure are explained in the text. The vertical dashed band covers the spectral range where the scattered pump light dominates over the white light probe; c) Schematic representation of the pump perturbation induced to the electronic band structure of a 2D perovskite and the expected line shape of a typical transient spectra. Here we define E_g , E_b , and ω as the bandgap, the exciton binding energy and the excitonic resonance of the unperturbed system, respectively, and E'_g , E'_b , and ω' the bandgap, the exciton binding energy and the excitonic resonance of the excited system, respectively; ΔE_g , ΔE_b , and δ indicate the electronic bandgap renormalization, the exciton binding energy renormalization and their difference, respectively.

also partially affected by Pauli blocking and phase space-filling as a consequence of the change of the electronic occupation in the system.^[77,78] For these reasons, the sign and amplitude of δ depend on the pump-probe delay as well as on temperature and chemical composition of the material, in our case on n . This scheme does not consider the contributions of the reflectivity due to the changes in the refractive index induced by the excitation that could distort the line shape of the transient signal.^[36,79]

With these considerations in mind, it is possible to discuss in detail the features of the TA spectra of DAMAPI-1 acquired at 77 K, reported in Figure 3b. The TA spectra show a PB1 minimum at energy (2.57 eV) higher than that measured at RT (2.51 eV), due to the contraction of the crystal structure favored by the increasing of the out-of-plane tilt angle of the octahedra induced by the lowering of the temperature that induces an increase of the lattice potential and hence of the electronic bandgap E_g .^[80,81] Moreover, the TA spectra acquired at 77 K, although qualitatively very similar to those acquired at RT (Figure 3a), present a clear difference. Indeed, the TA spectra at 77 K show a well-defined and intense bleaching signal (PB2) at 3.02 eV. The attribution of PB2 will be discussed later in the text when we will compare the experimental results with the theory. The absence of the PB2 signal at RT is probably due to the fact that the overall TA signal at RT is weaker than at 77 K and PB2 remains hidden within the PIA signal. The apparent change of the PIA line shape is of course due to the clearer presence of the PB2 peak and to the overall change of the transient signal intensity and linewidth by changing the temperature.

In order to better understand the experimental results of DAMAPI-1 we have performed DFT and excited-state simulations of its band structure and steady-state optical properties. Due to the very large number of atoms in the unit cell, the ab initio GW and BSE simulations of the full system are not feasible with the available computational tools and resources. Therefore, as described in the Experimental Section, we built up a simplified system (Cs_2PbI_4) to estimate the role of many-body effects, such as self-energy and excitonic terms in DAMAPI. DFT-KS band structures of the 2D perovskite having DA and Cs respectively as spacers are shown in Figure 4a.

The comparison shows a strong similarity between the DFT-KS band structures of the two systems around the band gap region, suggesting that the substitution of the organic spacer with Cs atoms, at this level of theoretical approximation, does not significantly change the band structure close to the bandgap (see also the partial density of states reported in Figure S4, Supporting Information).

On the basis of these findings, we performed the G_0W_0 calculation^[82] on the Cs_2PbI_4 model system and a wide bandgap opening, from 1.67 to 3.25 eV, is observed with an almost rigid blue shift of the conduction band and with an enhanced dispersion of the valence bands (see Figure 4b). According to our recent works on shorter organic spacer RPPs, i.e., BA_2PbI_4 (BA = butylammonium, $\text{CH}_3(\text{CH}_2)_2\text{NH}_3^+$), an underestimation of ≈ 0.3 eV is expected for the electronic gap.^[12,83] According to the two opposite contributions (see Section 2, Supporting Information for details) we expect a reasonable range for the true electronic gap

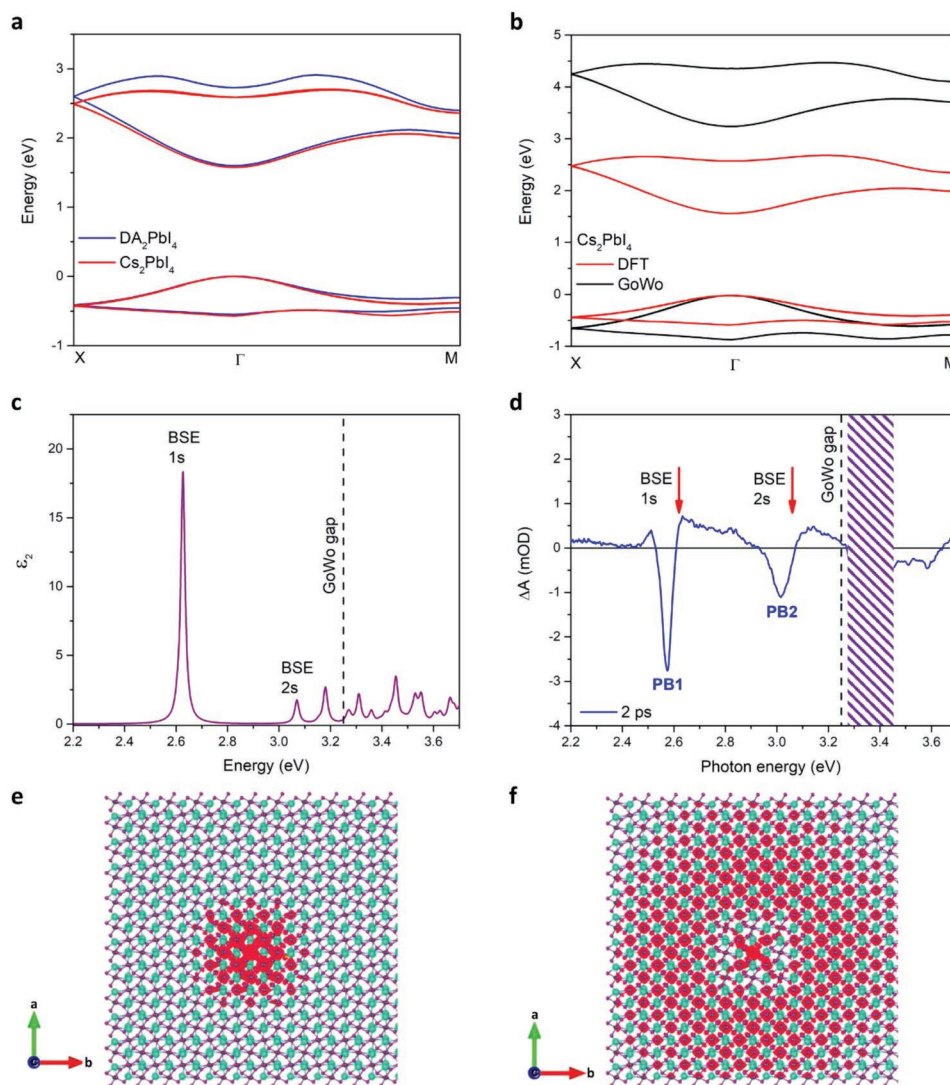


Figure 4. a) DFT-KS band structure of the Pb-based single sheet $n = 1$ 2D perovskite by using DA (red) and Cs (blue) as the spacer; b) DFT-KS (black) and GW (red) band structure obtained by Cs_2PbI_4 2D perovskite; c) BSE optical spectra for light polarized in-plane; d) Experimental TA of DAMAPI-1 acquired at 77 K and at the time delay of 2 ps and the theoretical evaluation of the energies of the excitons with 1s and 2s by BSE and the electronic bandgap by G_0W_0 (the vertical dashed band covers the spectral range where the scattered pump light dominates over the white light probe). Plot of the modulus square of the excitonic wavefunction of DAMAPI $n = 1$ for e) 1s and f) 2s excitons.

from 3.25 to 3.55 eV. This energy range matches the broad negative signal in the range of 3.3–3.6 eV observed in the TA spectra collected at 77 K (Figure 3b) and partially covered by the scattered light of the pump. At this point, the evaluation of the excitonic binding energy was performed by an ab initio BSE approach. Figure 4c reports the imaginary part of the dielectric constant of Cs_2PbI_4 obtained considering the electric field polarized in the plane of the lead iodide octahedra, with the aim to simulate our actual FTAS experimental condition (Figure S5, Supporting Information also reports the results obtained polarizing the electric field out of plane). The energies of the bright excitonic optical peaks near to the band edge at the Γ , Z points for the first (at 2.62 eV) and second (at 3.06 eV) principal quantum number, n , suggest the assignment of PB1 to the 1s exciton and of PB2 to the 2s exciton. The excitonic fine structure of the bright and dark excitons is reported and discussed in detail in Section S3

(Supporting Information). Consistently with recent literature on similar perovskites,^[59,84] the first exciton is a dark state with a bright-dark splitting of ≈ 20 meV. Additionally, several dark excitons are present at higher energies and near the second bright exciton.

The square modulus of the excitonic wavefunctions at 2.62 and 3.06 eV, reported in Figure 4e,f, shows their 1s and 2s character, respectively. In fact, both square moduli display a spherical shape and a node is present for the 2s (Figure 4f). The analysis in terms of single-particle transitions (see Figure S3, Supporting Information in Section S3) of all bright and dark excitons below 3.5 eV, shows that they originate only from transitions from VBM to CBM at Γ and Z point or k-points in their proximity. In particular, both 2s, assigned to PB2 (Figure S3d, Supporting Information) and 1s, assigned to PB1 (Figure S3a, Supporting Information), involve only Gamma and Z points.

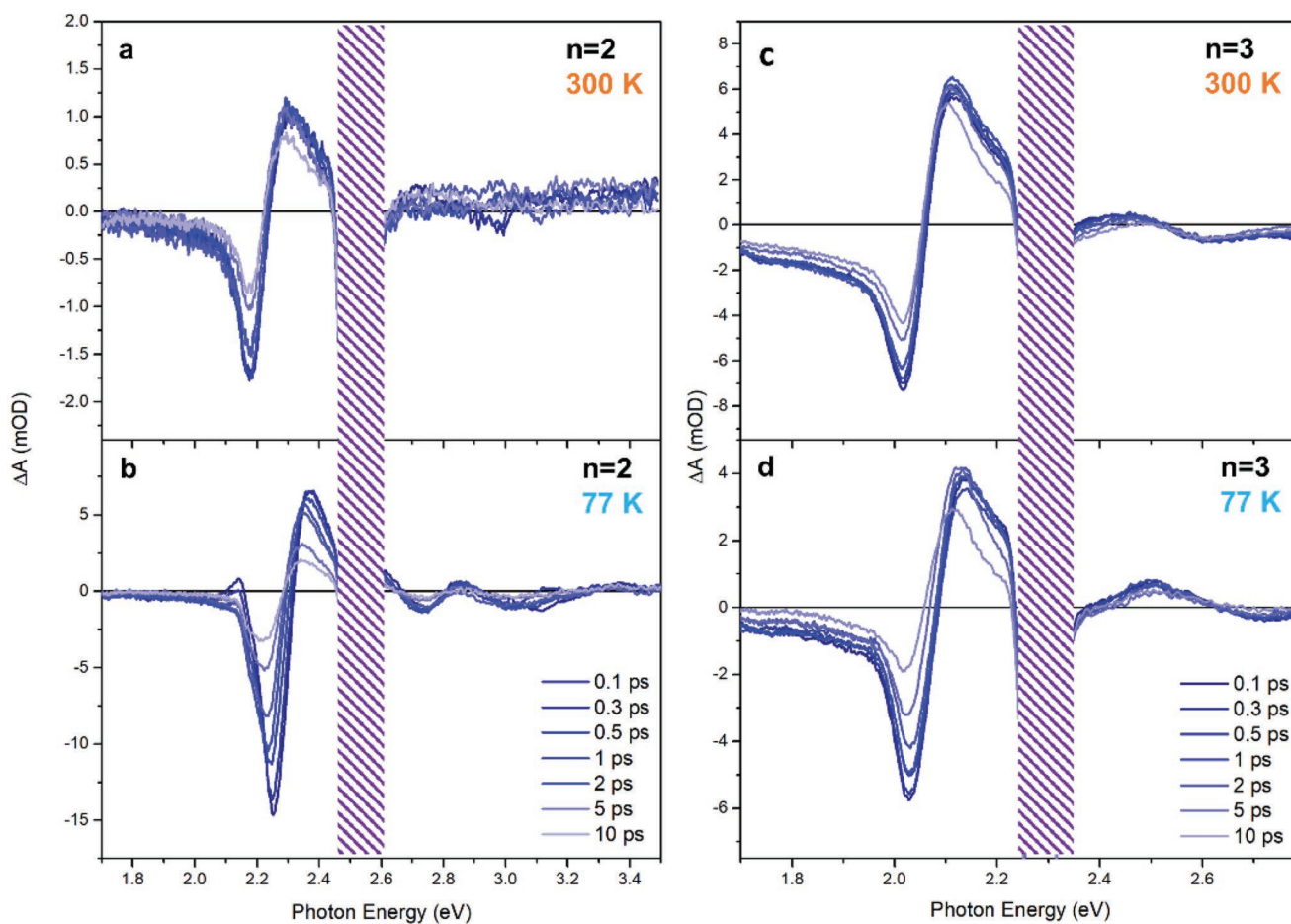


Figure 5. TA spectra of DAMAPI-2 acquired at selected time delays with $E_p = 2.50$ eV at a) RT and b) 77 K. TA spectra of DAMAPI-3 acquired at selected time delays with energy pump of 2.25 eV at c) RT and d) 77 K.

The good agreement between the theoretical results and the experimental TA data is shown in Figure 4d where the energies of the excitons with 1s and 2s and the electronic bandgap are reported together with the TA spectra of DAMAPI-1 acquired at 77 K and $t = 2$ ps. In fact, the BSE spectrum, calculated for the Cs_2PbI_4 , succeeds in well reproducing the absolute energy values for excitons 1s and 2s and, more importantly, it perfectly matches their energy difference of 440 meV. It is indeed well known that the position of the BSE calculated optical peaks are quite insensitive to the presence of different dielectric screening (such as due to different organic spacers or substrates) and specifically for a similar 2D perovskites (BA_2PbI_4) uncertainty of the binding energy estimation of the order of hundreds of meV has been found.^[85] It is important to note that the experimental TA spectra only give approximate energies of the excitons or the electronic bandgap, mainly because of the derivative-like shape of the transient signals and their width. Within those limits, the experimental data allow us to assign a marked 1s and 2s character to the PB1 and PB2 signals, respectively.

Because of the difficulty of calculating the band structure for $l > 1$, we will discuss the TA spectra acquired for multilayer perovskites with $n = 2$ (DAMAPI-2) and $n = 3$ (DAMAPI-3) using the assignment obtained for $n = 1$. The TA spectra taken at RT and 77 K are shown in Figure 5 for selected time delays

($t = 0.1, 0.2, 0.5, 1.0, 2.0, 5.0,$ and 10.0 ps). The TA spectra of DAMAPI-2 at RT present (Figure 5a) an intense PB1 at 2.17 eV and a PIA in the energy range 2.25–2.50 eV. The minimum of the PB1 is at lower energies than that of the PB1 in DAMAPI-1 at the same temperature (Figure 3a) and the energy difference is in line with the values obtained with other 2D systems.^[3,39,80] This confirms that the sample is principally composed of $n = 2$ sheets that induce a smaller quantum confinement than $n = 1$ and therefore have smaller E_b and E_g .

The TA spectra of DAMAPI-2 taken at 77 K (Figure 5b) show a PB1 at slightly higher energy (2.22 eV) than that acquired at RT (2.17 eV). This behavior is in line with what is found in literature in which the increase of the exciton absorption energy with the lowering of the temperature is negligible for systems with $l > 1$.^[80] The assignment of the PB signals at higher energies (2.75 and 3.00 eV) is uncertain but based on the typical excitonic binding energies for similar 2D systems it is reasonable that the PB at 2.75 eV could be related to the electronic bandgap and the negative band centered at 3.00 eV to transitions involving higher (lower) conduction (valence) bands at Γ point or different critical points. Analogous considerations and attributions are also valid for the TA spectra reported in Figure 5c,d and measured in DAMAPI-3 that show an intense PB signal at about 2.02 eV at RT and 77 K.

3.1. Dynamics of the Transient Absorption

The decay dynamics of PB1 and PB2 were analyzed as a function of excitation fluence, sample temperature, and number of perovskite layers, investigating how the composition of the 2D perovskite systems affects the observed EEA, which is a non-radiative many-body interaction, where the kinetic energy of an exciton is transferred to another exciton.^[86] It is conventionally described as a bimolecular process and has been demonstrated to be dominant in other materials with reduced dimensionality^[17,87,88] as well as in other 2D perovskites.^[46,89] We analyze the data using a simple model that also takes into account decay channels that are independent of the exciton density and include all the radiative and non-radiative recombination (such as trapping by defects and impurities) that take place in a temporal window of the order of hundreds of picoseconds or nanoseconds. The density-independent mechanisms come into play when the EEA loses efficiency as the exciton density decreases with time. The experimental data were fit with the following formula:

$$\Delta A(t) = \left(\frac{\Delta A_0}{1 + \frac{t}{\tau}} + \Delta A_1 \right) \cdot \left(1 + \operatorname{erf} \left(\frac{t}{\rho} \right) \right) \quad (1)$$

where $\Delta A(t)$ is the transient intensity expressed in OD at a defined time delay, ΔA_0 is the initial transient intensity, τ is the EEA decay time and ΔA_1 is a constant that considers all the recombination processes that last for more than 1 ns and ρ is the signal rise time. The EEA decay time τ extracted from the curve fitting is directly correlated to the EEA rate constant by the following formula:

$$\frac{1}{\tau} = n_0 k \quad (2)$$

where n_0 is the photoexcited exciton density and k is the EEA rate constant. Here we want to point out that the EEA decay time becomes faster as the exciton density increases, which is the typical behavior of a scattering process. In order to study the generation and decay of excitons, we selected the pump photon energies almost resonant with the 1s excitonic transition and with an excess of energy similar for all the investigated samples. In **Figure 6a** we report the PB1 dynamics for DAMAPI-1 at 77 K with $E_p = 2.75$ eV collected at different excitation fluences (220, 660, and 1650 $\mu\text{J cm}^{-2}$) and hence different photoexcited carrier densities ($2.4, 7.3$ and $18 \times 10^{13} \text{ cm}^{-2}$, details in Section S5, Supporting Information). The experimental data (see Figure S7, Supporting Information) are fit using Equation (1) and show a decay time that is inversely proportional to the excitation density, as expected from Equation (2). Under the given experimental conditions, we determine the EEA rate constant for DAMAPI-1 to be $k = (1.2 \pm 0.2) \times 10^{-2} \text{ cm}^2 \text{ s}^{-1}$ (all the details are

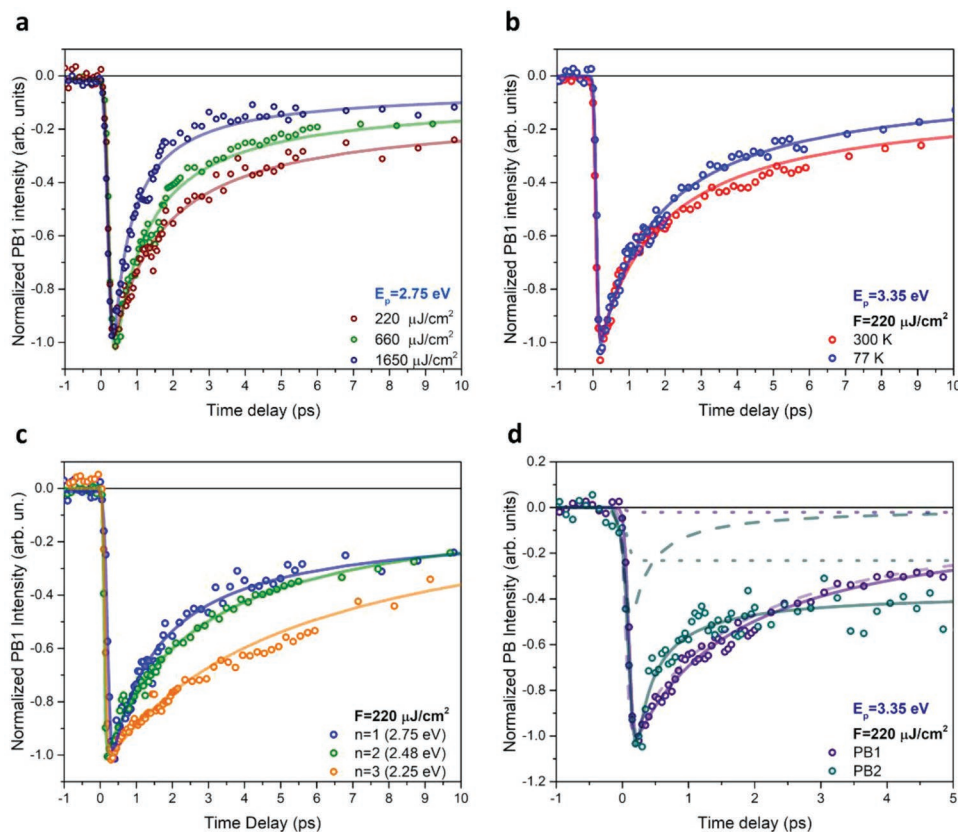


Figure 6. a) PB1 of DAMAPI-1 at 77 K and with excitation at 2.75 eV at different fluences. b) PB1 of DAMAPI-1 at 77 K and RT with excitation at 3.35 eV. c) PB1 of DAMAPI-1, DAMAPI-2, DAMAPI-3 at 77 K and with the similar excess of excitation energy at 220 $\mu\text{J cm}^{-2}$. d) PB1 and PB2 of DAMAPI-1 at 77 K and with excitation at 3.35 eV with a fluence of 220 $\mu\text{J cm}^{-2}$.

discussed in Section S5, Supporting Information). This result is in line with the values already obtained for other 2D materials such as MoS₂ in $(4.3 \pm 1.1) \times 10^{-2} \text{ cm}^2 \text{ s}^{-1}$ ^[90] and for RPPs with butylammonium as the spacer $(1.7 \pm 0.5) \times 10^{-2} \text{ cm}^2 \text{ s}^{-1}$.^[47] The EEA rate constants are very similar to the values found for RPPs having butylammonium and dodecylammonium, suggesting that the organic spacer only slightly affects the EEA rate. Although the exciton binding energies of DAMAPI-1 and MoS₂ are similar ($\approx 600 \text{ meV}$), the EEA rate constant is lower for the RPP system with respect to the MoS₂. This behavior can be explained by considering that the EEA rate constant strongly depends on the effective dielectric screening of the material that is higher for perovskites (≈ 5)^[91] than for MoS₂ (≈ 3).^[92]

In Figure 6b we report the PB1 dynamics for DAMAPI-1 at RT and 77 K with $E_p = 3.35 \text{ eV}$ at $220 \mu\text{J cm}^{-2}$ together with the best fit obtained using Equation (1). The experimental data clearly show that the exciton lifetime becomes longer as the temperature increases. The physical meaning of this result can be manifold. In analogy with the microscopic theory of the EEA process in MoS₂, the effect of the temperature is to widen the energy distribution of the excitons. It follows that the low temperatures facilitate the EEA because they favor the population of excitons having small momentum.^[47] This trend is in agreement with an EEA process that lasts longer at higher temperature because of the increase of the crystal dimension due to the thermal expansion and of the thermal vibrations of the lattice that reduce the EEA efficiency. We cannot exclude that this trend is also emphasized by the increase of 2D perovskite absorption at low temperature that determines an increase of the exciton density and hence an enhancement of the scattering rate. These results are in agreement with those collected with $E_p = 2.75 \text{ eV}$ and reported in Figure S6 (Supporting Information).

Figure 6c shows the decay dynamics of PB1 in samples with different layers (DAMAPI-1, DAMAPI-2 and DAMAPI-3) at the same fluence ($220 \mu\text{J cm}^{-2}$) and pumped respectively at 2.75, 2.50, and 2.25 eV, with the aim to excite them with a similar excess of energy with respect to the excitonic transitions. The data, reported together with the best fit, show that exciton lifetimes become longer as the number of perovskite layer increases. A higher number of layers reduces the quantum confinement as well as the exciton concentration at equal total number of photoexcited excitons with the ensuing reduction of the EEA efficiency,^[93] while diffusion is favored. **Table 1** summarizes the time constants and EEA rate constants for DAMAPI-1, DAMAPI-2, and DAMAPI-3.

Finally, Figure 6d shows the PB1 and PB2 dynamics for DAMAPI-1 acquired at 77 K with $E_p = 3.35 \text{ eV}$ and a fluence

Table 1. Decay time τ and estimated EEA rate k for DAMAPI-1, DAMAPI-2, and DAMAPI-3 at the PB1 energies. The details on the estimation of k for DAMAPI-2 and DAMAPI-3 are discussed in Section S5 (Supporting Information).

Number of Layers (n)	$T = 77 \text{ K}, F = 220 \mu\text{J cm}^{-2}$		
	1	2	3
PB1 energy (eV)	2.75	2.48	2.25
τ (ps)	1.4 ± 0.2	2.4 ± 0.2	3.7 ± 0.3
k ($10^{-2} \text{ cm}^2 \text{ s}^{-1}$)	1.2 ± 0.2	0.7 ± 0.3	0.4 ± 0.2

of $220 \mu\text{J cm}^{-2}$. The energy of the pump is above both the 1s and 2s excitonic resonances. In this case, we find that in the first picoseconds the dynamics of the two exciton resonances differ significantly, in particular, the 2s exciton shows a shorter decay time constant (0.40 ps) than 1s (1.50 ps). The larger physical size of the 2s wavefunction should make the EEA more efficient and, furthermore, decay channels of this excited state into states at lower energies compete to make the decay of PB2 faster in the first picosecond. Therefore, we cannot assign an EEA constant rate to 2s as its dynamics are influenced by other interfering decay processes. At delay times above 2 ps, we find a long decay dynamic for both PB1 and PB2 with time constants of hundreds of picoseconds. While this long decay time can be easily attributed to recombination of the 1s exciton, for 2s it could be explained by the interaction with dark excitonic states with energies closer to the bright excitonic state, as identified by the BSE calculations (see Section S2, Supporting Information).

4. Conclusion

In this work we have reported transient absorption measurements on the 2D perovskite DAMAPI (DA₂MA_{*n*-1}PbI_{3*n*+1}), with DA = CH₃-(CH₂)₁₁-NH₃⁺ as a spacer, obtaining both spectral and temporal information about excitonic absorption and decay. In particular, the derivative character of the transient absorption signals has allowed us to observe electronic transitions involving the formation of excitons with principal quantum numbers 1s and 2s. The interpretation of the data is supported by theoretical calculations of the electronic and optical features based on GW and BSE approaches.

The analysis of the decay of the transient absorption signal has shown that at the excitation fluences used for the experiments, the process that dominates the decay of the absorption bleaching of the excitonic resonances at short delay times is the exciton–exciton annihilation mechanism, of which we have determined the constant rates.

Finally, we wish to point out that transient absorption measurements not only allow the study of the dynamics of the excited carriers but, because of their high sensitivity to the changes in the carrier density induced by the excitation, they also allow the observation of spectral features otherwise not observable with steady-state measurements.

Acknowledgements

Open Access Funding provided by Consiglio Nazionale delle Ricerche within the CRUI-CARE Agreement.

Conflict of Interest

The authors declare no conflict of interest.

Author Contributions

F.M., L.D.M., and D.C. conceived the project. G.A., D.C., P.O.K., S.T., and A.P. performed the transient measurements. G.A. performed the analysis

of the transient results with the help and supervision of D.C. L.D.M., M.D.G., and M.C. synthesized the material, performed the steady-state measurements, and also wrote the related Experimental Section. M.P., G.G., and G.A. performed the theoretical calculations and wrote the theoretical section. All experimental and theoretical results were discussed among all the authors. D.C. and G.A. wrote the first draft of the manuscript and all authors contributed to writing, reviewing, and editing the manuscript to its final form.

Data Availability Statement

The data that support the findings of this study are available from the corresponding author upon reasonable request.

Supporting Information

Supporting Information is available from the Wiley Online Library or from the author.

Keywords

2D materials, excitons, perovskites, quasi-2D perovskites, Ruddlesden-Popper perovskites, transient absorption spectroscopy

Received: August 11, 2022
Revised: November 17, 2022
Published online:

- [1] L. Mao, C. C. Stoumpos, M. G. Kanatzidis, *J. Am. Chem. Soc.* **2019**, *141*, 1171.
- [2] G. Grancini, M. K. Nazeeruddin, *Nat. Rev. Mater.* **2019**, *4*, 4.
- [3] J.-C. Blancon, J. Even, C. C. Stoumpos, M. G. Kanatzidis, A. D. Mohite, *Nat. Nanotechnol.* **2020**, *15*, 969.
- [4] I. C. Smith, E. T. Hoke, D. Solis-Ibarra, M. D. McGehee, H. I. Karunadasa, *Angew. Chem., Int. Ed.* **2014**, *53*, 11232.
- [5] G. Grancini, C. Roldàn-Carmona, I. Zimmermann, E. Mosconi, X. Lee, D. Martineau, S. Narbey, F. Oswald, F. De Angelis, M. Graetzel, M. K. Nazeeruddin, *Nat. Commun.* **2017**, *8*, 15684.
- [6] X. Zhang, G. Wu, W. Fu, M. Qin, W. Yang, J. Yan, Z. Zhang, X. Lu, H. Chen, *Adv. Energy Mater.* **2018**, *8*, 1702498.
- [7] Y. Huang, Y. Li, E. L. Lim, T. Kong, Y. Zhang, J. Song, A. Hagfeldt, D. Bi, *J. Am. Chem. Soc.* **2021**, *143*, 3911.
- [8] M. Yuan, Li Na Quan, R. Comin, G. Walters, R. Sabatini, O. Voznyy, S. Hoogland, Y. Zhao, E. M. Beauregard, P. Kanjanaboos, Z. Lu, D. Ha Kim, E. H. Sargent, *Nat. Nanotechnol.* **2016**, *11*, 872.
- [9] K. Wang, J. Y. Park, Akriti, L. Dou, *EcoMat* **2021**, *3*, e12104.
- [10] Ke-Z Du, Q. Tu, Xu Zhang, Q. Han, J. Liu, S. Zauscher, D. B. Mitzi, *Inorg. Chem.* **2017**, *56*, 9291.
- [11] Li Na Quan, B. P. Rand, R. H. Friend, S. G. Mhaisalkar, T.-W. Lee, E. H. Sargent, *Chem. Rev.* **2019**, *119*, 7444.
- [12] G. Giorgi, K. Yamashita, M. Palummo, *J. Phys. Chem. Lett.* **2018**, *9*, 5891.
- [13] M. Palummo, S. Postorino, C. Borghesi, G. Giorgi, *Appl. Phys. Lett.* **2021**, *119*, 051103.
- [14] G. Giorgi, K. Yamashita, M. Palummo, *J. Mater. Chem. C* **2018**, *6*, 10197.
- [15] M. Palummo, E. Berrios, D. Varsano, G. Giorgi, *ACS Energy Lett.* **2020**, *5*, 457.
- [16] A. Ramasubramaniam, *Phys. Rev. B* **2012**, *86*, 115409.
- [17] A. Chernikov, T. C. Berkelbach, H. M. Hill, A. Rigosi, Y. Li, B. Aslan, D. R. Reichman, M. S. Hybertsen, T. F. Heinz, *Phys. Rev. Lett.* **2014**, *113*, 076802.
- [18] K. Leng, I. Abdelwahab, I. Verzhbitskiy, M. Telychko, L. Chu, W. Fu, X. Chi, Na Guo, Z. Chen, Z. Chen, C. Zhang, Q.-H. Xu, J. Lu, M. Chhowalla, G. Eda, K. P. Loh, *Nat. Mater.* **2018**, *17*, 908.
- [19] X. Gan, Ou Wang, K. Liu, X. Du, L. Guo, H. Liu, *Sol. Energy Mater. Sol. Cells* **2017**, *162*, 93.
- [20] Z. He, Y. Liu, Z. Yang, J. Li, J. Cui, D. Chen, Z. Fang, H. He, Z. Ye, H. Zhu, N. Wang, J. Wang, Y. Jin, *ACS Photonics* **2019**, *6*, 587.
- [21] G. Wu, T. Yang, X. Li, N. Ahmad, X. Zhang, S. Yue, J. Zhou, Y. Li, H. Wang, X. Shi, S. (F.) Liu, K. Zhao, H. Zhou, Y. Zhang, *Matter* **2021**, *4*, 582.
- [22] Q. Cao, P. Li, W. Chen, S. Zang, L. Han, Y. Zhang, Y. Song, *Nano Today* **2022**, *43*, 101394.
- [23] S. Bellani, A. Bartolotta, A. Agresti, G. Calogero, G. Grancini, A. Di Carlo, E. Kymakis, F. Bonaccorso, *Chem. Soc. Rev.* **2021**, *50*, 11870.
- [24] A. Z. Chen, M. Shiu, J. H. Ma, M. R. Alpert, D. Zhang, B. J. Foley, D.-M. Smilgies, S.-H. Lee, J. J. Choi, *Nat. Commun.* **2018**, *9*, 1336.
- [25] Y. Gao, Z. Wei, P. Yoo, E. Shi, M. Zeller, C. Zhu, P. Liao, L. Dou, *J. Am. Chem. Soc.* **2019**, *141*, 15577.
- [26] J. Chen, J. Y. Seo, N. G. Park, *Adv. Energy Mater.* **2018**, *8*, 1702714.
- [27] K. T. Cho, G. Grancini, Y. Lee, E. Oveisi, J. Ryu, O. Almora, M. Tschumi, P. A. Schouwink, G. Seo, S. Heo, J. Park, J. Jang, S. Paek, G. Garcia-Belmonte, M. K. Nazeeruddin, *Energy Environ. Sci.* **2018**, *11*, 952.
- [28] R. Lin, J. Xu, M. Wei, Y. Wang, Z. Qin, Z. Liu, J. Wu, Ke Xiao, B. Chen, So M Park, G. Chen, H. R. Atapattu, K. R. Graham, J. Xu, J. Zhu, L. Li, C. Zhang, E. H. Sargent, H. Tan, *Nature* **2022**, *603*, 73.
- [29] S. Sun, M. Lu, X. Gao, Z. Shi, X. Bai, W. W. Yu, Yu Zhang, *Adv. Sci.* **2021**, *8*, 2102689.
- [30] M. Ban, Y. Zou, J. P. H. Rivett, Y. Yang, T. H. Thomas, Y. Tan, T. Song, X. Gao, D. Credgington, F. Deschler, H. Siringhaus, B. Sun, *Nat. Commun.* **2018**, *9*, 3892.
- [31] Li Zhang, C. Sun, T. He, Y. Jiang, J. Wei, Y. Huang, M. Yuan, *Light Sci Appl* **2021**, *10*, 61.
- [32] L. Schmidt-Mende, V. Dyakonov, S. Olthof, F. Ünlü, K. M. T. Lê, S. Mathur, A. D. Karabanov, D. C. Lupascu, L. M. Herz, A. Hinderhofer, F. Schreiber, A. Chernikov, D. A. Egger, O. Shargaieva, C. Cocchi, E. Unger, M. Saliba, M. M. Bryanvand, M. Kroll, F. Nehm, K. Leo, A. Redinger, J. Höcker, T. Kirchartz, J. Warby, E. Gutierrez-Partida, D. Neher, M. Stollerfoht, U. Würfel, M. Unmüssig, et al., *APL Mater.* **2021**, *9*, 109202.
- [33] O. F. Williams, Z. Guo, J. Hu, L. Yan, W. You, A. M. Moran, *J. Chem. Phys.* **2018**, *148*, 134706.
- [34] J. Yin, P. Maity, M. De Bastiani, I. Dursun, O. M. Bakr, J.-L. Brédas, O. F. Mohammed, *Sci. Adv.* **2017**, *3*, e1701793.
- [35] C. Wang, Y. Liu, X. Feng, C. Zhou, Y. Liu, Xi Yu, G. Zhao, *Angew. Chem., Int. Ed.* **2019**, *58*, 11642.
- [36] M. B. Price, J. Butkus, T. C. Jellicoe, A. Sadhanala, A. Briane, J. E. Halpert, K. Broch, J. M. Hodgkiss, R. H. Friend, F. Deschler, *Nat. Commun.* **2015**, *6*, 8460.
- [37] D. Catone, G. Ammirati, P. O'Keeffe, F. Martelli, L. Di Mario, S. Turchini, A. Paladini, F. Toschi, A. Agresti, S. Pescetelli, A. Di Carlo, *Energies* **2021**, *14*, 708.
- [38] X. Wu, M. T. Trinh, X.-Y. Zhu, *J. Phys. Chem. C* **2015**, *119*, 14714.
- [39] Z. Gan, X. Wen, C. Zhou, W. Chen, F. Zheng, S. Yang, J. A. Davis, P. C. Tapping, T. W. Kee, H. Zhang, B. Jia, *Adv. Opt. Mater.* **2019**, *7*, 1900971.
- [40] E. P. Booker, T. H. Thomas, C. Quarti, M. R. Stanton, C. D. Dashwood, A. J. Gillett, J. M. Richter, A. J. Pearson, N. J. L. K. Davis, H. Siringhaus, M. B. Price, N. C. Greenham, D. Beljonne, S. E. Dutton, F. Deschler, *J. Am. Chem. Soc.* **2017**, *139*, 18632.

- [41] R. L. Milot, R. J. Sutton, G. E. Eperon, A. A. Haghighirad, J. Martinez Hardigree, L. Miranda, H. J. Snaith, M. B. Johnston, L. M. Herz, *Nano Lett.* **2016**, *16*, 7001.
- [42] J. Cho, J. T. Dubose, P. V. Kamat, *J. Phys. Chem. Lett.* **2020**, *11*, 2570.
- [43] J. Yin, P. Maity, R. Naphade, B. Cheng, Jr-H He, O. M. Bakr, J.-L. Brédas, O. F. Mohammed, *ACS Nano* **2019**, *13*, 12621.
- [44] D. Lin, L. Ma, W. Ni, C. Wang, F. Zhang, H. Dong, G. G. Gurzadyan, Z. Nie, *J. Mater. Chem. A* **2020**, *8*, 25402.
- [45] J. Yin, O. M. Bakr, O. F. Mohammed, *J. Phys. Chem. C* **2021**, *125*, 9630.
- [46] S. Deng, E. Shi, L. Yuan, L. Jin, L. Dou, L. Huang, *Nat. Commun.* **2020**, *11*, 664.
- [47] A. Steinhoff, F. Jahnke, M. Florian, *Phys. Rev. B* **2021**, *104*, 155416.
- [48] M. Cinquino, A. Fieramosca, R. Mastria, L. Polimeno, A. Moliterni, V. Olieric, N. Matsugaki, R. Panico, M. De Giorgi, G. Gigli, C. Giannini, A. Rizzo, D. Sanvitto, L. De Marco, *Adv. Mater.* **2021**, *33*, 2102326.
- [49] M. Cinquino, L. Polimeno, G. Lerario, M. De Giorgi, A. Moliterni, V. Olieric, A. Fieramosca, S. Carallo, R. Mastria, V. Ardizzone, L. Dominici, D. Ballarini, C. Giannini, D. Sanvitto, A. Rizzo, L. De Marco, *J. Lumin.* **2020**, *221*, 117079.
- [50] D. Catone, L. Di Mario, F. Martelli, P. O’Keeffe, A. Paladini, J. Stefano Pelli Cresi, A. K. Sivan, L. Tian, F. Toschi, S. Turchini, *Nanotechnology* **2020**, *32*, 025703.
- [51] J. S. Pelli Cresi, L. Di Mario, D. Catone, F. Martelli, A. Paladini, S. Turchini, S. D’Addato, P. Luches, P. O’Keeffe, *J. Phys. Chem. Lett.* **2020**, *11*, 5686.
- [52] G. Kresse, J. Hafner, *Phys. Rev. B* **1993**, *48*, 13115.
- [53] G. Kresse, J. Hafner, *Phys. Rev. B* **1994**, *49*, 14251.
- [54] G. Kresse, J. Furthmüller, *Comput. Mater. Sci.* **1996**, *6*, 15.
- [55] G. Kresse, J. Furthmüller, *Phys. Rev. B* **1996**, *54*, 11169.
- [56] J. P. Perdew, K. Burke, M. Ernzerhof, *Phys. Rev. Lett.* **1996**, *77*, 3865.
- [57] S. Grimme, J. Antony, S. Ehrlich, H. Krieg, *J. Chem. Phys.* **2010**, *132*, 154104.
- [58] S. Grimme, S. Ehrlich, L. Goerigk, *J. Comput. Chem.* **2011**, *32*, 1456.
- [59] M. R. Filip, D. Y. Qiu, M. Del Ben, J. B. Neaton, *Nano Lett.* **2022**, *22*, 4870.
- [60] P. Giannozzi, O. Andreussi, T. Brumme, O. Bunau, M. Buongiorno Nardelli, M. Calandra, R. Car, C. Cavazzoni, D. Ceresoli, M. Cococcioni, N. Colonna, I. Carnimeo, A. Dal Corso, S. De Gironcoli, P. Delugas, R. A. Distasio, A. Ferretti, A. Floris, G. Fratesi, G. Fugallo, R. Gebauer, U. Gerstmann, F. Giustino, T. Gorni, J. Jia, M. Kawamura, H.-Y. Ko, A. Kokalj, E. Küçükbenli, M. Lazzeri, et al., *J. Phys. Condens. Matter* **2017**, *29*, 465901.
- [61] P. Giannozzi, O. Baseggio, P. Bonfà, D. Brunato, R. Car, I. Carnimeo, C. Cavazzoni, S. De Gironcoli, P. Delugas, F. Ferrari Ruffino, A. Ferretti, N. Marzari, I. Timrov, A. Urru, S. Baroni, *J. Chem. Phys.* **2020**, *152*, 154105.
- [62] A. Marini, C. Hogan, M. Grüning, D. Varsano, *Comput. Phys. Commun.* **2009**, *180*, 1392.
- [63] D. Sangalli, A. Ferretti, H. Miranda, C. Attacalite, I. Marri, E. Cannuccia, P. Melo, M. Marsili, F. Paleari, A. Marrazzo, G. Prandini, P. Bonfà, M. O. Atambo, F. Affinito, M. Palummo, A. Molina-Sánchez, C. Hogan, M. Grüning, D. Varsano, A. Marini, *J. Phys. Condens. Matter* **2019**, *31*, 325902.
- [64] G. Strinati, H. J. Mattausch, W. Hanke, *Phys. Rev. B* **1982**, *25*, 2867.
- [65] G. Strinati, *Riv. Nuovo Cimento Soc. Ital. Fis.* **1988**, *11*, 1.
- [66] W. Hanke, L. J. Sham, *Phys. Rev. Lett.* **1974**, *33*, 582.
- [67] W. Hanke, L. J. Sham, *Phys. Rev. B* **1980**, *21*, 4656.
- [68] G. Onida, L. Reining, A. Rubio, *Rev. Mod. Phys.* **2002**, *74*, 601.
- [69] X. Jiang, Q. Zheng, Z. Lan, W. A. Saidi, X. Ren, J. Zhao, *Sci. Adv.* **2021**, *7*, eabf3759.
- [70] S. Ismail-Beigi, S. G. Louie, *Phys. Rev. Lett.* **2003**, *90*, 076401.
- [71] S. Ismail-Beigi, S. G. Louie, *Phys. Rev. Lett.* **2005**, *95*, 156401.
- [72] Z. Ji, H. Hong, J. Zhang, Qi Zhang, W. Huang, T. Cao, R. Qiao, C. Liu, J. Liang, C. Jin, L. Jiao, K. Shi, S. Meng, K. Liu, *ACS Nano* **2017**, *11*, 12020.
- [73] H. Wang, J. Bang, Y. Sun, L. Liang, D. West, V. Meunier, S. Zhang, *Nat. Commun.* **2016**, *7*, 11504.
- [74] S. Meng, E. Kaxiras, *J. Chem. Phys.* **2008**, *129*, 054110.
- [75] Q. Zheng, W. A. Saidi, Yu Xie, Z. Lan, O. V. Prezhdo, H. Petek, J. Zhao, *Nano Lett.* **2017**, *17*, 6435.
- [76] W. R. Duncan, O. V. Prezhdo, *Annu. Rev. Phys. Chem.* **2007**, *58*, 143.
- [77] E. A. A. Pogna, M. Marsili, D. De Fazio, S. Dal Conte, C. Manzoni, D. Sangalli, D. Yoon, A. Lombardo, A. C. Ferrari, A. Marini, G. Cerullo, D. Prezzi, *ACS Nano* **2016**, *10*, 1182.
- [78] S. Schmitt-Rink, D. S. Chemla, D. A. B. Miller, *Phys. Rev. B* **1985**, *32*, 6601.
- [79] J. Liu, J. Leng, S. Wang, J. Zhang, S. Jin, *J. Phys. Chem. Lett.* **2019**, *10*, 97.
- [80] J.-C. Blancon, A. V. Stier, H. Tsai, W. Nie, C. C. Stoumpos, B. Traoré, L. Pedesseau, M. Kepenekian, F. Katsutani, G. T. Noe, J. Kono, S. Tretiak, S. A. Crooker, C. Katan, M. G. Kanatzidis, J. J. Crochet, J. Even, A. D. Mohite, *Nat. Commun.* **2018**, *9*, 2254.
- [81] Y. P. Varshni, *Physica* **1967**, *34*, 149.
- [82] T. Galvani, F. Paleari, H. P. C. Miranda, A. Molina-Sánchez, L. Wirtz, S. Latil, H. Amara, F. Ducastelle, *Phys. Rev. B* **2016**, *94*, 125303.
- [83] C. Quarti, G. Giorgi, C. Katan, J. Even, M. Palummo, *Adv. Opt. Mater.*, <https://doi.org/10.1002/adom.202202801>.
- [84] K. Posmyk, N. Zawadzka, M. Dyksik, A. Surrente, D. K. Maude, T. Kazimierzczuk, A. Babinski, M. R. Molas, W. Paritmongkol, M. Maczka, W. A. Tisdale, P. Plochocka, M. Baranowski, *J. Phys. Chem. Lett.* **2022**, *7*.
- [85] A. Molina-Sánchez, *ACS Appl. Energy Mater.* **2018**, *1*, 6361.
- [86] A. Suna, *Phys. Rev. B* **1970**, *1*, 1716.
- [87] N. Kumar, Q. Cui, F. Ceballos, D. He, Y. Wang, H. Zhao, *Phys. Rev. B* **2014**, *89*, 125427.
- [88] L. Valkunas, Y.-Z. Ma, G. R. Fleming, *Phys. Rev. B* **2006**, *73*, 115432.
- [89] G. Delport, G. Chehade, F. Lédée, H. Diab, C. Milesi-Brault, G. L. Trippé-Allard, J. Even, J.-S. Lauret, E. Deleporte, D. Garrot, *J. Phys. Chem. Lett.* **2019**, *10*, 5153.
- [90] D. Sun, Yi Rao, G. A. Reider, G. Chen, Y. You, L. Brézin, A. R. Harutyunyan, T. F. Heinz, *Nano Lett.* **2014**, *14*, 5625.
- [91] D. Marongiu, M. Saba, F. Quochi, A. Mura, G. Bongiovanni, *J. Mater. Chem. C* **2019**, *7*, 12006.
- [92] D. Y. Qiu, F. H. Da Jornada, S. G. Louie, *Phys. Rev. B* **2016**, *93*, 235435.
- [93] L. Yuan, L. Huang, *Nanoscale* **2015**, *7*, 7402.